Tether Dynamics and Vibration Analysis

R.L. Engelstad and E.G. Lovell

October 1987

UWFDM-728

Presented at the PSN/NASA/ESA Second International Conference on Tethers in Space, 4–8 October 1987, Venice, Italy.

FUSION TECHNOLOGY INSTITUTE

UNIVERSITY OF WISCONSIN

MADISON WISCONSIN

Tether Dynamics and Vibration Analysis

R.L. Engelstad and E.G. Lovell

Fusion Technology Institute
University of Wisconsin
1500 Engineering Drive
Madison, WI 53706

http://fti.neep.wisc.edu

October 1987

UWFDM-728

Presented at the PSN/NASA/ESA Second International Conference on Tethers in Space, 4–8 October 1987, Venice, Italy.

TETHER DYNAMICS AND VIBRATION ANALYSIS

R. L. Engelstad* and E. G. Lovell
Fusion Technology Institute
University of Wisconsin-Madison

Abstract

An assessment is made of the effects of tension gradients on the free vibrations of tethers. A perturbation procedure is developed in general terms. Specific cases considered include centrifugal loading and distributions from gravity gradients. Results indicate that such gradients can significantly alter natural frequencies, with changes nearly independent of wave number. Distortions in mode shapes also occur but are less severe. Node points and maximum amplitudes are shifted in the direction of decreasing tension.

Equations of motion are presented for flow-induced vibrations in tethers used for fluid transfer, such as propellants and coolants. Response curves are obtained by numerical integration. It has been found that if the flow has a pulsating characteristic, large amplitude displacements are likely to develop over a wide range of system parameters.

I. Introduction

Mechanical vibrations can naturally occur in tether systems designed for a variety of applications. One of the most important influences on vibrations of such flexible members is internal tension, which may change considerably because of large unsupported lengths. An objective of this work is to determine the effects of tension gradients on free vibrations. This is a necessary prerequisite for forced vibration analysis by modal procedures.

Tethers may also function as fluid lines for the transfer of propellants, contaminated liquids, coolants, etc. It is important to be able to determine the dynamic response and identify the influence of factors such as fluid velocity, fluctuating flow, tether stiffness and effective tension. These issues are considered in the work which follows.

II. Tension Gradient Effects on the Free Vibrations of Tethers

For basic problems in which the tension T and mass per unit length ρ are functions of the axial coordinate, x, the equation of motion for the transverse displacement component v is

$$\frac{\partial}{\partial x}\left\{T(x)\,\frac{\partial v}{\partial x}\right\} = \rho(x)\left[\frac{\partial^2 v}{\partial t^2} - v\Omega^2\right] \tag{1}$$

where t and Ω denote time and tether rotational speed, respectively. For small axial gradients, the following substitutions are made for T and ρ:

$$T(x) = T_o[1 + \delta(x)] \tag{2}$$

$$\rho(x) = \rho_o[1 + \varepsilon(x)] \,. \tag{3}$$

The form of the solution used for a typical modal component can be expressed as

$$v_n(x,t) = \left[V_n(x) + \sum_{m\neq n} a_m V_m(x)\right]\exp(i\omega_n t) \tag{4}$$

$$\omega_n^2 = \omega_n^{*2}(1+b_n) \,. \tag{5}$$

Here $V_n(x)$ and ω_n^* are solutions to the gradient-free problem, i.e.,

$$V_n(x) = \sin n\pi x/\ell \qquad n = 1,2,\ldots \tag{6}$$

$$\omega_n^{*2} = M_E(\Omega n\pi)^2/\rho_o\ell - \Omega^2 \tag{7}$$

where M_E represents a concentrated end mass. The coefficients a_m and b_n are small order terms and facilitate the development of the perturbation solution. These expressions are now substituted into the equation of motion, (1):

$$\begin{aligned}&[T_o V_n'' + \rho_o\Omega^2 V_n + \rho_o\omega_n^{*2}V_n] + T_o[\delta(x)V_n']' \\ &+ \rho_o\omega_n^{*2}[(1 + \Omega^2/\omega_n^{*2})\varepsilon(x) + b_n]V_n \\ &+ \sum_{m\neq n} a_m[T_o V_m'' + \rho_o\omega_n^{*2}(1 + \Omega^2/\omega_n^{*2})V_m] \\ &= -\rho_o\omega_n^{*2}\varepsilon(x)b_n V_n - T_o\sum_{m\neq n}[\delta(x)a_m V_m']' \\ &-\rho_o\omega^{*2}\sum_{m\neq n} a_m V_m[b_n + b_n\varepsilon(x) + \varepsilon(x) + \varepsilon(x)\Omega^2/\omega_n^{*2}] \,.\end{aligned} \tag{8}$$

The equation for first order perturbation terms is obtained by deleting the right side of (8):

$$\begin{aligned}&T_o[\delta(x)V_n']' + \rho_o\omega_n^{*2}[(1 + \Omega^2/\omega_n^{*2})\varepsilon(x) + b_n]V_n \\ &+ \sum_{m\neq n} a_m[T_o V_m'' + \rho\omega_n^{*2}(1 + \Omega^2/\omega_n^{*2})V_m] = 0 \,.\end{aligned} \tag{9}$$

Series coefficients a_m and b_n can be determined from the following expressions:

$$\begin{aligned}a_m = &\left[T_o\int_0^\ell [\delta(x)V_n']'V_m dx\right. \\ &\left. + \rho_o\omega_n^{*2}(1+\Omega^2/\omega_n^{*2})\int_0^\ell \varepsilon(x)V_n V_m dx\right]/ \\ &k_m\rho_o(1 + \Omega^2/\omega_n^{*2})(\omega_m^{*2} - \omega_n^{*2})\end{aligned} \tag{10a}$$

*Member AIAA

$$b_n = [-T_o/\rho_o k_n \omega_n^{*2}(1 + \Omega^2/\omega_n^{*2})] \int_0^{\ell} [\delta(x)V_n']'V_n dx$$

$$- (1/k_n) \int_0^{\ell} V_n^2 \varepsilon(x) dx \qquad (10b)$$

where

$$V_m''(x) = -\omega^{*2}(1 + \Omega^2/\omega_n^{*2})V_m(x)\rho_o/T_o \qquad (11)$$

$$k_m = \int_0^{\ell} V_m^2(x)\, dx \ . \qquad (12)$$

Centrifugal Tension Gradient

Consider an idealized example in which the axial gradient results from rotation only. The origin of coordinates is at the center of rotation, the length is ℓ and an end mass M_E has negligible relative displacement (as in some simple constellations). The mass per unit length is also constant. Thus

$$\varepsilon(x) = 0$$

$$T(x) = T_o[1 + \delta(x)]$$

$$= M_E \ell \Omega^2[1 + \rho_o(\ell^2 - x^2)/2M_E\ell] \ . \qquad (13)$$

The perturbation parameters follow from (10):

$$a_m = 2M_T(-1)^{m+n}mn(m^2+n^2)/$$

$$(1+\Omega^2/\omega^{*2})M_E\pi^2(m+n)^2(m-n)^2(m^2-n^2) \qquad (14)$$

$$b_n = (M_T/3M_E)(1-3/4n^2\pi^2) \qquad (15)$$

where M_T is the tether mass. From (15), the frequency change will be nearly the same for all modes. The percentage difference can be substantial, as shown in Fig. 1. Modifications in mode shapes are not as large. From Figs. 2-4, it can be seen that maximum amplitudes and node points are shifted in the direction of decreasing tension.

Gravity Gradient Tension Distribution

In this example, the model consists of a tether aligned with the local vertical having a lower end mass M_1 at r_1 and an upper end mass M_2 at r_2. Force equilibrium for the system requires

$$\Omega^2[M_2 r_2 + M_1 r_1 + M_T(r_2 + r_1)/2]$$

$$= GM[M_1/r_1^2 + M_2/r_2^2 + M_T/r_1 r_2] \qquad (16)$$

where GM is the gravitational constant of the earth. At a generic position r, the internal tether tension is

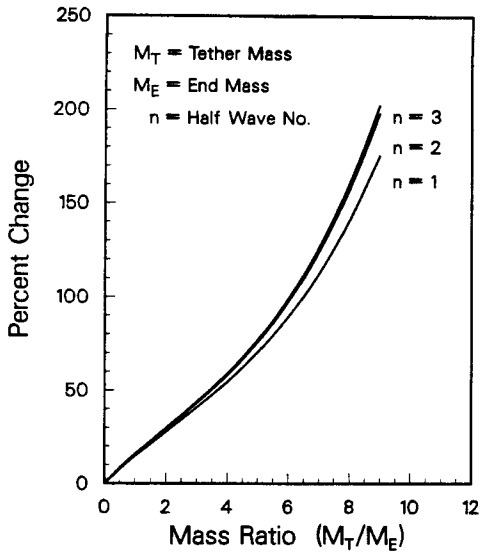

Fig. 1 Change in vibration frequencies of rotating tethers from added mass

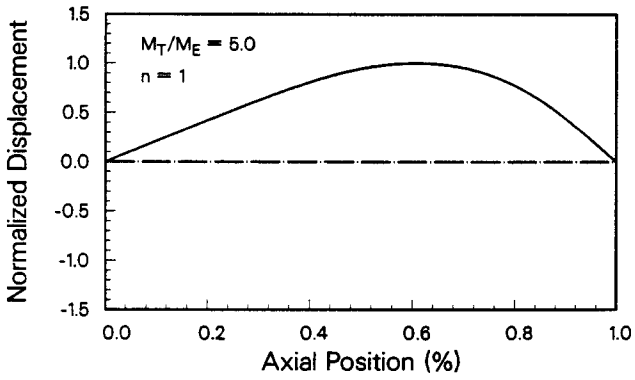

Fig. 2 Fundamental Mode of Rotating Tether With Added Mass.

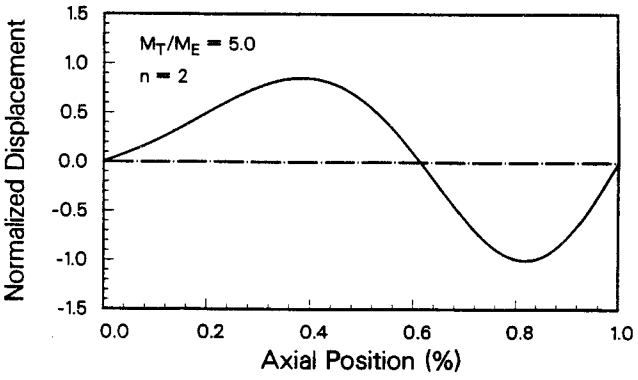

Fig. 3 Second Mode of Rotating Tether With Added Mass.

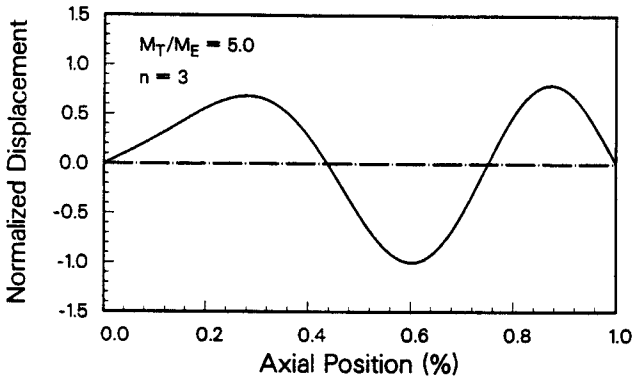

Fig. 4 Third Mode of Rotating Tether With Added Mass.

$$T(r) = \Omega^2 M_T(r_1^2 - r^2)/2\ell + GMM_T(1/r_1 - 1/r)/\ell + F_1 \quad (17)$$

where F_1 is the force difference acting on M_1,

$$F_1 = GMM_1/r_1^2 - M_1 r_1 \Omega^2 . \quad (18)$$

The modification in mode shapes and frequencies will have the same form as given in (4) and (5). However, the axial coordinate x will originate at mass M_1, i.e.,

$$x = r - r_1 . \quad (19)$$

Frequency correction coefficients depend upon all system parameters:

$$b_n = \frac{(M_T/2M_1)}{(1 - r_1^3\Omega^2/GM)} \{[1 - (\ell/r_1)(2/3 + 1/n^2\pi^2) + (\ell/r_1)^2(1/2 + 3/n^2\pi^2)] - (\Omega^2 r_1^3/GM)[1 - (\ell/r_1)(1/3 + 1/2\, n^2\pi^2)]\} . \quad (20)$$

For cases in which $\Omega^2 r_1^3/GM \ll 1$, this can be simplified:

$$b_n = (M_T/2M_1)[1 - (\ell/r_1)(2/3 + 1/n^2\pi^2) + (\ell/r_1)^2(1/2 + 3/n^2\pi^2)] . \quad (21)$$

It can be seen that the modification to the square of each natural frequency is essentially the same, i.e., one half of the ratio of tether mass to end mass. Numerical results are presented in Table 1.

Similarly the amplitude coefficients are obtained from (10a), i.e.,

$$a_m = 2\ell\, I/\pi^2(m^2 - n^2)(1 + \Omega^2/\omega_n^{*2})$$

Table 1. Percent Change in Natural Frequencies for Various Tether Length and Mass Ratios

n	ℓ/r_1	M_T/M_1=0.4	0.8	1.2
1	0.005	9.515	18.334	26.754
5	0.005	9.519	18.343	26.766
1	0.010	9.446	18.205	26.566
5	0.010	9.459	18.229	26.601
1	0.015	9.480	18.269	26.660
5	0.015	9.489	18.285	26.683

where

$$I = \int_0^\ell [\delta(x)V_n']'V_m dx$$

$$= (GMM_T/F_1\ell r_1^2 - M_T r_1\Omega^2/F_1\ell)mn[(n+m)^{-2} + (n-m)^{-2}]^*$$

$$+ (2GMM_T/F_1 r_1^3 + M_T\Omega^2/F_1)mn(-1)^{m+n}$$

$$\times (m^2+n^2)(n-m)^{-2}(n+m)^{-2} - (GMM_T\ell mn/F_1\pi^2 r_1^4)$$

$$\times \{\frac{[(n-m)^2\pi^2-2](-1)^{m+n} + 2}{(n-m)}$$

$$+ \frac{[(n+m)^2\pi^2 - 2](-1)^{m+n} + 2}{(n+m)^4}\} . \quad (22)$$

As with the preceding example, moderate distortion of the mode shapes will result for a wide range of numerical values of the parameters in (22).

III. Flow-Induced Vibrations

The model used consists of a completely flexible uniform tether of length ℓ, cross-sectional area A_T and mass per unit length ρ_T. The fluid velocity is c, cross-sectional flow area A_F and mass per unit length ρ_F. Gravity gradient and rotational effects are not included in the model. It is also assumed that nominal tube dimensions do not significantly change with pressurization and motion. The fluid is considered viscous and incompressible.

The undeformed centerline of the tether coincides with the x axis. Free and forced response of the tether is allowed in both the x-y and x-z planes along with longitudinal deformations. An effective axial force T_{EFF} includes the induced axial load from internal pressure. Nonlinear tension effects are accounted for by including higher order terms in the tether extension expression.

Equations of motion were developed using Hamiltons's principle and general variational calculus procedures. These equations follow for the axial, transverse and lateral directions:

*This group of terms is zero if m and n are both odd or both even.

$$(\rho_F + \rho_T)\frac{\partial^2 u}{\partial t^2} + \rho_F \frac{\partial c}{\partial t} + \kappa_o \rho_T \frac{\partial u}{\partial t} - EA_T \frac{\partial^2 u}{\partial x^2}$$

$$- \frac{\partial}{\partial x}\{(EA_T - T_{EFF})[\tfrac{1}{2}(\frac{\partial v}{\partial x})^2 + \tfrac{1}{2}(\frac{\partial w}{\partial x})^2$$

$$- (\frac{\partial u}{\partial x})(\frac{\partial v}{\partial x})^2 - (\frac{\partial u}{\partial x})(\frac{\partial w}{\partial x})^2]\} = 0 \qquad (23)$$

$$(\rho_F + \rho_T)\frac{\partial^2 v}{\partial t^2} + 2\rho_F c \frac{\partial^2 v}{\partial x \partial t} + \rho_F c^2 \frac{\partial^2 v}{\partial x^2}$$

$$+ \rho_F \frac{\partial c}{\partial t}\frac{\partial v}{\partial x} + \kappa_o \rho_T \frac{\partial v}{\partial t} - \frac{\partial}{\partial x}\{T_{EFF}\frac{\partial v}{\partial x}$$

$$+ (EA_T - T_{EFF})[\frac{\partial u}{\partial x} - (\frac{\partial u}{\partial x})^2$$

$$+ \tfrac{1}{2}(\frac{\partial v}{\partial x})^2 + \tfrac{1}{2}(\frac{\partial w}{\partial x})^2]\frac{\partial v}{\partial x}\} = 0 \qquad (24)$$

$$(\rho_F + \rho_T)\frac{\partial^2 w}{\partial t^2} + 2\rho_F c \frac{\partial^2 w}{\partial x \partial t} + \rho_F c^2 \frac{\partial^2 w}{\partial x^2}$$

$$+ \rho_F \frac{\partial c}{\partial t}\frac{\partial w}{\partial x} + \kappa_o \rho_T \frac{\partial w}{\partial t} - \frac{\partial}{\partial x}\{T_{EFF}\frac{\partial w}{\partial x}$$

$$+ (EA_T - T_{EFF})[\frac{\partial u}{\partial x} - (\frac{\partial u}{\partial x})^2$$

$$+ \tfrac{1}{2}(\frac{\partial v}{\partial x})^2 + \tfrac{1}{2}(\frac{\partial w}{\partial x})^2]\frac{\partial w}{\partial x}\} = 0 \qquad (25)$$

where E is the elastic modulus of the tether, κ_o is the damping coefficient, and u, v and w are the displacement components in the x, y and z directions, respectively.

By neglecting longitudinal inertia, (23) can be combined with (24) and (25) to eliminate the axial displacement component, u:

$$(\rho_F + \rho_T)\frac{\partial^2 v}{\partial t^2} + 2\rho_F c \frac{\partial^2 v}{\partial x \partial t} + \rho_F c^2 \frac{\partial^2 v}{\partial x^2} + \kappa_o \rho_T \frac{\partial v}{\partial t}$$

$$- T_{EFF}\frac{\partial^2 v}{\partial x^2} - \frac{EA_T}{2\ell}\frac{\partial^2 v}{\partial x^2}\int_0^{\ell}[(\frac{\partial v}{\partial x})^2 + (\frac{\partial w}{\partial x})^2]dx$$

$$+ \frac{\partial^2 v}{\partial x^2}\rho_F \frac{\partial c}{\partial t}(\ell/2 - x) = 0 \; . \qquad (26)$$

The companion equation in the z direction can be obtained by interchanging w and v. These partial differential equations are reduced to ordinary differential equations by Galerkin's method. The form of the solution is a summation of linear modes, i.e.,

$$v(x,t) = \sum_{n=1}^{\infty} v_n(x,t)\phi_n(x) = \sum_{n=1}^{\infty} v_n(t)\sin\frac{n\pi x}{\ell} \; .$$

Thus the corresponding equation of motion is

$$\ddot{v}_r + \frac{4\rho_F c}{\ell(\rho_F + \rho_T)}\sum_{n=1}^{\infty}\frac{2rn}{(r^2 - n^2)}\dot{v}_r$$

$$+ \frac{\kappa_o \rho_T}{(\rho_F + \rho_T)}\dot{v}_r + \frac{(T_{EFF} - \rho_F c^2)\pi^2 r^2}{\ell^2(\rho_F + \rho_T)}v_r$$

$$+ \frac{EA_T \pi^4 r^2}{4\ell^4(\rho_F + \rho_T)}v_r \sum_{m=1}^{\infty} m^2(v_m^2 + w_m^2)$$

$$- \frac{\rho_F \dot{c}}{\ell(\rho_F + \rho_T)}\sum_{n=1}^{\infty}\frac{8n^3 r}{(n^2 - r^2)}v_n = 0 \qquad (27)$$

where $(r \pm n)$ is odd, otherwise the two series in (27) are zero. The fluid velocity is denoted by c. In the case of flow with a pulsating component, the representation is

$$c = c_o(1 + \mu \cos \lambda t) \; . \qquad (28)$$

For numerical purposes, dimensionless variables are defined as follows:

$$\bar{v} = v/\ell, \quad \bar{w} = w/\ell, \quad \bar{t} = \omega_1 t \qquad (29)$$

$$\omega_r^2 = (T_{EFF} - \rho_F c_o^2)\pi^2 r^2/(\rho_F + \rho_T)\ell^2 \; . \qquad (30)$$

Computational Results

Tether dynamic response for multiple modes was determined by a Runge-Kutta integration routine. Approximately 6000 time steps per cycle were used. For both examples the harmonic coefficient (μ) was 0.40, damping was 1% and the length was 100 m. In the first case, shown in Fig. 5, a fluid velocity of 1 m/s is low enough that steady state motion characterizes the response. However, as seen from Fig. 6, an increase in speed to 5 m/s causes an unstable response with midspan displacements growing exponentially. Generally the nature of the time histories is quite sensitive to changes in system parameters.

IV. CONCLUSIONS

A perturbation procedure has been outlined for use in the vibration analysis of tethers having mass or tension gradients. When applied to the cases of tension variations from rotation or gravity gradients, it has been shown that vibration frequencies can be significantly changed. Asymmetries occur in mode shapes characterized by shifts in locations of maximum values and node points toward low tension regions. Equations of motion have also been developed for flow-induced vibrations of tethers. Results indicate that if the velocity has a harmonic variation, large amplitude motion is possible over a wide range of physical parameters.

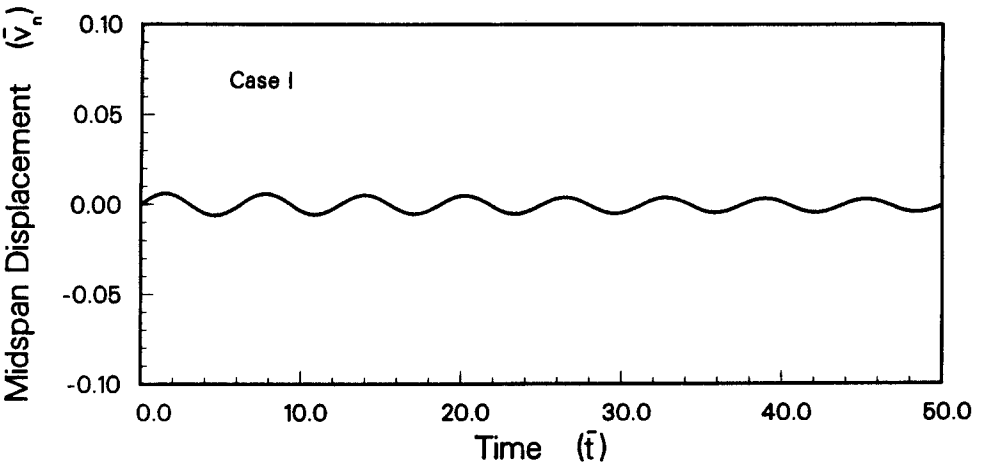

Fig. 5 Maximum Tether Displacement From Low Speed Flow-Induced Vibration.

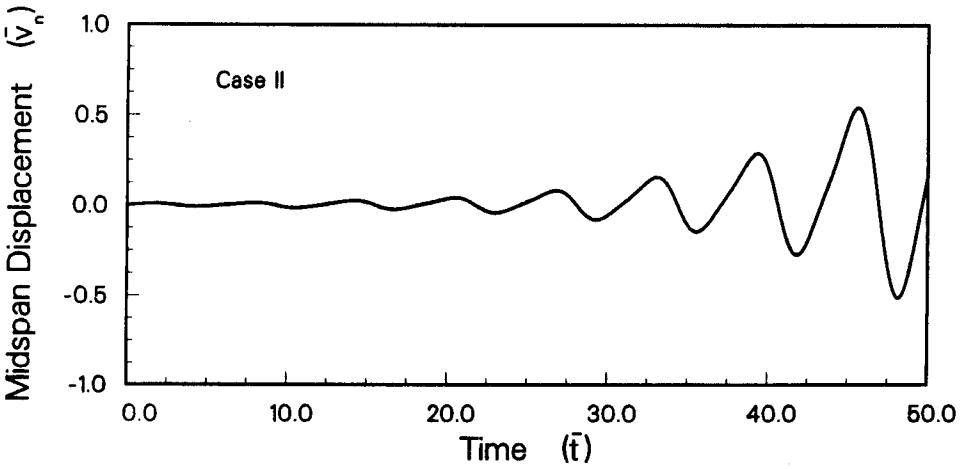

Fig. 6 Maximum Tether Displacement From High Speed Flow-Induced Vibration.

Acknowledgment

Support for this work has been provided by the University of Wisconsin, NASA, and the Wisconsin Electric Utilities Research Foundation.